

FELES: A New 2D Software Design Tool for Optoelectronic Devices

Gen Lin TAN, Keith LEE, and J.M. XU

Department of Electrical Engineering, University of Toronto, Toronto,
Canada M5S 1A4

FELES is a new two dimensional finite element optoelectronic device simulator that self-consistently solves the electrical equations (Poisson's and the electron and hole continuity equations), the optical wave equation, the photon rate equation, and the thermal conduction equation simultaneously for devices of any arbitrary geometry and different material compositions. The simulation tool can be used for proof-of-concept and evaluation of device operation, and assist in the optimization and design of device structure.

1. Introduction

In the past decade, the structure of high performance lasers has become increasingly sophisticated. In order to reduce the development time and the costly expense of device fabrications, it is becoming evident that accurate versatile laser device models are needed for proof-of-concept and evaluation of new device and to assist in the optimization of device design. FELES (Finite Element Light Emitter Simulator) is a new general purpose software tool that can perform these tasks. This two-dimensional model self-consistently solves Poisson's equation, the electron and hole current continuity equations, the optical wave equation, the thermal conduction equation, and the photon rate equation for laser devices. The features of FELES-1, comparing with other laser simulators[1-3], are: (1)It uses the finite element method to discretize the electrical equations, the thermal conduction equation, and the optical wave equation in a unified way. Due to the flexibility of the finite element method, FELES can simulate various laser devices with arbitrary geometry, doping and composition, and is suitable for exploring new device structures. (2)It uses a series of highly efficient algorithms such that the 2D finite element analysis for laser devices can be carried out in a workstation environment rather than on supercomputers like [1-3]. This makes FELES a design tool that is more available to widespread users. (3)It incorporates more complete physical models to account for most of the important physical processes and effects. The results from the simulations of conventional laser devices have been compared with our experimental measurements and have been found to be in good agreement. (4)It has a convenient input format and procedure[4] which can describes any complicated device structure easily and a post-procesor which can provide 3-D distribution profile and contour map and any cross-section distribution figure of any physical quantities inside the simulated device structure. This gives good

insights into physical processes involved.

2. Device model

FELES is based on the following six non-linear differential equations:

$$\nabla \cdot \epsilon \nabla \psi = -q(p - n + N_D^+ - N_A^-), \quad (1)$$

$$\frac{\partial n}{\partial t} = \frac{1}{q} \nabla \cdot J_n + (G - R) \quad (2)$$

$$\frac{\partial p}{\partial t} = -\frac{1}{q} \nabla \cdot J_p + (G - R). \quad (3)$$

$$\nabla \cdot (-\kappa T) + \rho_m c \frac{\partial T}{\partial t} = F \cdot J + E_g R_{nr}, \quad (4)$$

$$\nabla^2 E(x, y) + (k_0 \bar{n}^2 - \beta^2) E(x, y) = 0 \quad (5)$$

$$\frac{dS_p}{dt} = \left(\frac{c_0}{n_{eff}} G_p - \frac{1}{\tau_{ph}} \right) S_p + C \tilde{R}_{sp}. \quad (6)$$

The electrical model (eqs.(1)-(3)) includes Fermi-Dirac statistics, position dependent band structure and incomplete ionization. Moreover, it takes into account doping, temperature, composition and electrical field dependent mobilities, and bulk, surface, Auger, spontaneous emission, and stimulated emission recombinations. Under non-isothermal condition, an additional thermal diffusion current component, which arises from temperature gradients, is included in the current density J_n and J_p , in addition to the conventional drift component and diffusion component of current.

The thermal model involves solving of the thermal conduction equation(eq.(4)) under given thermal boundary conditions. It considers two thermal sources: the Joule heat and the non-radiative recombination heat. It incorporates various lattice-temperature dependent physical parameters including temperature dependent thermal conductivity (κ), band structure, and carrier statistics.

The optical model consists of solving the wave equation(eq.(5)) and it is coupled with the electrical and the thermal models through the photon rate equation(eq.(6)). β is the modal propagation constant, and \bar{n} is the complex refractive index given by:

$$\bar{n}^2(x,y) = \bar{n}_0^2 + (-\alpha_R + j) \frac{\bar{n}_0 g(x,y)}{k_0} - j \frac{\bar{n}_0}{k_0} (c_n n + c_p p) \quad (7)$$

where $j = \sqrt{-1}$, \bar{n}_0 is the bulk refractive index, α_R is the line width broadening factor, $g(x,y)$ is the local peak gain and $(c_n n + c_p p)$ is the free carrier absorption. In this model, the local gain is calculated taking into account the k-selection rules, the reduced density of states including discrete energy levels and continuous energy spectrum, and broadening effects due to intraband relaxation [6],

$$g = \max[\bar{C}(E_i) \sum_J \sum_n \int_{E_g + E_{cn} + E_{vn}}^{\infty} \rho_r^J \cdot M_J^2 [f_{cn}^J - f_{vn}^J] L(E) dE] \quad (8)$$

where the index J refers to either $J = hh$ heavy hole or $J = lh$ light hole, $\bar{C}(E_i) = (0.5 h e^2) / (m_0^2 n_r \epsilon_0 c E_i)$, E_i is the photon energy, n_r the effect refractive index of the MQW structure, ρ_r^J the reduced density of states, M_J the dipole matrix element, $L(E)$ the Lorentzian function, and f_{cn}^J, f_{vn}^J the Fermi functions of the conduction band and the valence band, respectively. In eq.(8), for energies below the barrier height, the reduced density of states is given by step function and for energies above the barrier height, by the square root of the energy. Although g can be calculated directly using quasi-Fermi potentials obtained from 2-D analysis, it would take long cpu time. We use a pre-processor to calculate the peak gain as a function of carrier concentration and find an approximate analytical fitting formula around threshold gain. At this stage of the model development, FELES allows the choices of the linear gain approximation or a higher-power polynomial. The spontaneous emission rate(in eq.(6)) is calculated from the following formula[7]

$$R_{sp} = \sum_{i,j} \int_0^{\infty} \bar{C}(E) M_{ij}^2 \rho(E) D(E) f_{c_j} (1 - f_{v_i}) dE \quad (9)$$

3. Simulation Algorithm

With the use of conventional computation methods, the simulations of a laser device would require excessively fine mesh and exceedingly large data storage and cpu time, and often result in non convergence. To overcome these difficulties, new computation methods are needed. In FELES, we used three new numerical techniques: a new finite element discretization method, called FE-QSG (i.e. the S-G scheme embedded in the quadrature of a finite element method), which has higher accuracy and better convergence than the conventional finite element method(FE) [9]. Thus, the new discretization method can use a coarser mesh for a given accuracy than that required by the conventional FE or the BIM-SG method in a finite difference scheme; A new self-adaptive mesh refinement technique[6], which automatically creates denser grid points at the interfaces and in the transition regions where charge or field change drastically and improves conver-

gence considerably; A new preconditioning iteration method named ILUV-CGS[10], solving the linear and non-linear equations more efficiently, which employs an Incomplete LU decomposition by Value (ILUV) in conjunction with the CGS iteration scheme.

In solving the wave equation, the FE-QSG discretization method is used for the first time so that a higher accuracy solution on a coarser mesh can be obtained. Moreover we developed a generalized Rayleigh quotient-inverse iteration algorithm(RQIIM) to solve the generalized eigenvalue equation obtained from finite element discretization of the wave equation so that the solving of wave equation only needs tens seconds on a workstation (less than the cpu time for solving the Poisson equation once). It is well known that the eigenvalue problem is difficult and consumes a large amount of cpu time in general, and this is the reason why some laser simulators only use effective index approximation to solve wave equation[1-2].

Under non-isothermal conditions, the problem is more complicated and the convergence is a more serious problem because carrier statistics is exponentially dependent on the lattice-temperature. So iteration strategy must be selected carefully. A two-fold nested loops in FELES is adapted: first solving electrical equations at a fix temperature distribution (which is the previous temperature solution) to obtain an adiabatic approximation solution, then solving the thermal conduction equation to get new temperature distribution, and then repeat above loops until it converges. With this method, we avoid instability due to temperature variation. In the iteration procedure, the treatment of the rate equation(i.e. how to adjust the photon density), is very important. We use the information of dS/dG obtained in iteration, to self-adaptedly adjust the photon density so that the number of re-solving the wave equation is decreased to 2-3 per bias point of device.

4. Applications/Results

FELES has been used to study both AlGaAs/GaAs and InP/InGaAsP ridge waveguide laser diodes and the results showed good agreement with available experimental data. The program has also been used to study thermal effects on the threshold and quantum efficiency of lasers [11] under non-isothermal condition.

As a particular example of the application of the simulation software, the results of a recent utilization of the tool in evaluating the design and performance of a new Ridge Waveguide AlGaAs/GaAs Double-Heterojunction Lateral Current Injection laser structure (RWG-DH-LCI) are shown in Fig.1-4. Fig.1 shows fundamental optical mode and its contour plot. From the figure, we see that the optical confinement is very good in both dimensions. Fig.2 gives the electron density distribution at $V=0.6$ V which shows the electrons concentrate almost entirely in the active layer, but the concentration reduces quickly from the N^+ terminal to the P^+ terminal at low bias level. At the threshold of lasing, the distributions of n and p in the active layer are rather flat (Fig.3) which show the overlap of the modal field and the gain region is also good for the lateral injection structure. The current in the structure does not flow through any non-active region so that the parasitic loss and non-radiative recombination reduce dramatically

compared to the vertical injection counterpart. This is why the structure has a low threshold current (6 mA) and a high quantum efficiency. Fig.3 gives detailed $n(y)$ and $p(y)$ along the active layer at four biases above the threshold of lasing. $n(y)$ is almost equal to $p(y)$ in the active channel and increases on the P^+ side with bias. This is a result of the combination of non-linear recombinations, the great disparity in electron and hole mobilities, the ambipolar diffusion and the charge neutrality. Fig.4 shows the emission power versus current from one cleaved facet with reflectivity of 0.3 of a $300 \mu\text{m}$ long device.

The post-processor has compiled the simulated outputs into a series of graphical images to generate a motion-picture that shows the evolution of the device operation under bias current. A selection of frames from the movie [12] are shown in Fig.1-4 for demonstration.

REFERENCES

- [1] T. Ohtosh, etc., *Solid-State Electron.*, 30(1987) 627.
- [2] K.B. Kahen, *IEEE J. Quantum Electron.*, 24(1988) 641.
- [3] M. Ueno, etc., *IEEE J. Quan. Electron.*, 26(1990) 972-981.
- [4] G.L. Tan and J.M. Xu, *FELES User Manual*, Optoelectronics Lab, University of Toronto, 1992.
- [5] G.L. Tan, X.L. Yuan, Q.M. Zhang, W. Ku, and A. Shey, *IEEE Trans. on CAD/ICAS*, 8(1989) 468.
- [6] M. Rosenzweig, etc., *IEEE J. of Quan. Electron.*, 27(1991) 1804.
- [7] R.H. Yan, etc., *IEEE J. Quan. Electron.*, 26(1990) 213.
- [8] G.L. Tan, Q.M. Zhang, and J.M. Xu, *IEEE Trans. Magnetics*, 27(1991) 4158.
- [9] G.L. Tan, X.L. Yuan, Q.M. Zhang, W. Ku, and A. Shey, *IEEE Trans. on CAD/ICAS*, 8(1989)(1989) 468.
- [10] Z.Y. Zhao, Q.M. Zhang, G.L. Tan, and J.M. Xu, *IEEE Trans. CAD-ICS*, 11(1991) 1432.
- [11] G.L. Tan, N. Bewtra, K. Lee and J.M. Xu, submitted to *IEEE J. of Quantum Electronics*.
- [12] G.L. Tan, M. Lee, J.M. Xu, "6-minute movie for operation of Ridge Waveguide AlGaAs/GaAs Double-Heterojunction LCI laser", April, 1992.

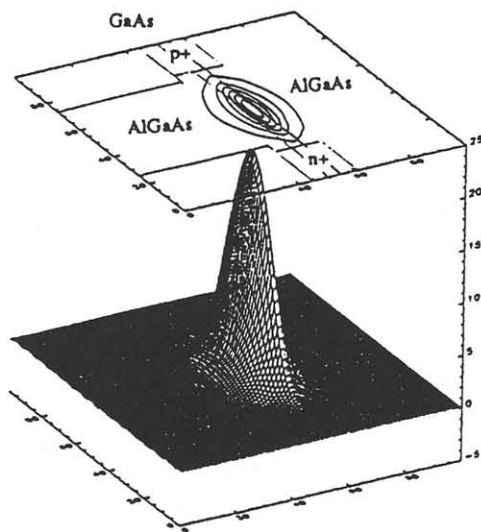


figure 1. fundamental optical mode and its contour plot.

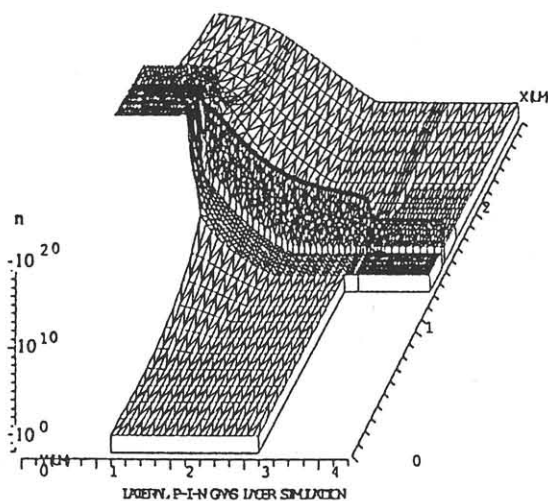


figure 2. electron concentration in device at $V = 0.6 \text{ V}$.

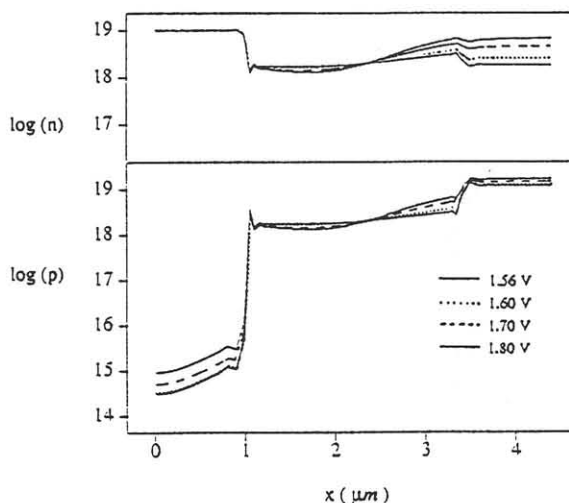


figure 3. electron and hole concentrations in active layer at different bias.

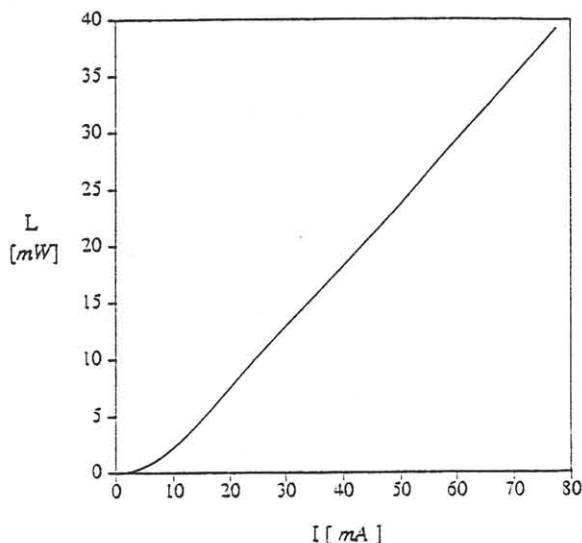


figure 4. simulated power-current (L-I) curve.